UNIVERSITY OF OKLAHOMA
GRADUATE COLLEGE

EXAMINING MID-LEVEL STABLE LAYERS OVER THE TROPICAL ATLANTIC DURING ORCESTRA

A THESIS
SUBMITTED TO THE GRADUATE FACULTY
in partial fulfillment of the requirements for the
Degree of
MASTER OF SCIENCE

by MACINTYRE M SYRETT

Norman, Oklahoma

2026

Downloaded from SHAREOK. Persistent Handle URL: https://hdl.handle.net/11244/342826

EXAMINING MID-LEVEL STABLE LAYERS OVER THE TROPICAL ATLANTIC DURING ORCESTRA

A THESIS APPROVED FOR THE
SCHOOL OF METEOROLOGY

BY THE COMMITTEE CONSISTING OF

Dr. James Ruppert Jr. (Chair)

Dr. Jason Furtado

Dr. Naoko Sakaeda

©Copyright by MACINTYRE M SYRETT 2026

All Rights Reserved.

Acknowledgments

This project was supported by the National Science Foundation (NSF) under Grant 2331200 (MMS, JHR), 2331199 (AAW), and 2331202 (MMB). I would like to thank Dr. Allison Wing and Dr. Michael Bell for their contributions to this thesis. We would like to thank Hans Segura and Hauke Schmidt for their initial insights into the existence and distribution of mid-level stable layers as observed on board the R/V Meteor, as well as the many other members of the ORCESTRA community who provided comments and feedback at various group workshops and discussions. ORCESTRA was made possible thanks to the support of the Max Planck Society (MPG), the European Research Council through Grant No. 101098063, the German Research Foundation (DFG), the German Aerospace Center (DLR), the German Federal Ministry for Education and Research (BMBF), the French National Centre for Scientific Research (CNRS), the Dutch Research Council (NWO), the European Space Agency (ESA), and the US National Science Foundation (NSF)

Table of Contents

Acknowledgments iv

List of Figures vi

Abstract viii

1 Introduction 1

2 Data and Methods 5

3 Results 7
3.1 Initial Sounding Observations and CFADs 7
3.2 The Relationship with Humidity 8
3.3 Comparison of Stable Layer Occurrence Across Campaigns 15
3.4 Mechanism-Denial Testing With a Radiative Transfer Model 17

4 Summary and Conclusions 21

Reference List 23

List of Figures

3.1 a) Example Skew–T log–P diagram taken from the R/V Meteor during ORCESTRA, showing a strong mid-level stable layer (inversion) and a rapid decrease in humidity across that layer (∼6 km). b) CFAD of $d\theta/dz$ with temperature as the vertical coordinate for all ORCESTRA soundings. The mean $d\theta/dz$ is shown in red. c) Same as b), but with altitude as the vertical coordinate. d) CFAD of relative humidity for all ORCESTRA soundings. The mean relative humidity profile is shown in green. Dashed lines in the CFADs correspond to local maxima objectively identified, a selection of which are incorporated into the Skew–T. 8

3.2 Scatter plot of the relationship between relative humidity layer difference (%) and the stability index ς (in K/km) for ORCESTRA observations. Each green point represents an individual measurement, with histograms along the margins showing the distributions of both variables. Negative relative humidity layer difference values indicate drier air above the stable layer. The "Example Sounding" denotes the sounding used in Figs. 3.1 and 3.8. 10

3.3 A selection of soundings with extremely strong mid-level stable layers from the ORCESTRA campaign. All soundings featured have values of $\varsigma \geq 15$ K km^{-1}. Note the presence of mid-level rapid vertical drying collocated with strong static stability in all soundings. 11

3.4 Same as Fig. 3.2, but for the DYNAMO campaign and without an example sounding. 12

3.5 Same as Fig. 3.4, but for the EUREC^{4}A campaign. 13

3.6 Same as Fig. 3.4, but for the OTREC campaign. 14

3.7 Vertical distribution of high-stability atmospheric layers across four field campaigns. Horizontal bars show the occurrence frequency of stable layers at different altitudes between 1–10 km, as occurrence normalized by total number of soundings (shown as N). The vertical axis is limited to 10 km since dropsonde datasets frequently lack data above this level. 16

3.8 Vertical profiles from mechanism denial experiments using the example R/V Meteor sounding from Fig. 3.1a. The left column shows $d\theta/dz$, the middle column displays relative humidity in green and mixing ratio in blue, and the right column shows longwave, shortwave, and net heating rates calculated by RRTMG. The solid yellow line indicates the shortwave heating rate averaged over a 24 hour period of solar angles. Row a) shows these values for the unaltered sounding profile. Row b) shows these profiles for heavily smoothed temperature and humidity profiles, but with the humidity structure near the stable layer preserved. It also shows the impact of imposing the net heating rate onto the smoothed potential temperature profile. Row c) is the same, but with the temperature structure preserved instead. 19

Abstract

Here we investigate elevated stable layers that frequently appeared at an altitude near 6 km in soundings obtained during the ORCESTRA field campaign. This observation is in conflict with the existing literature, which suggests that tropical stable layers are instead collocated with the 0°C level at around 4-5 km. Our analysis demonstrates a strong relationship between mid-level stability and the change in relative humidity across the stable layer (decreasing upwards). Mechanism-denial tests with an infrared radiative transfer model support the hypothesis that vertical changes in relative humidity layer lead to differential radiative heating rates, thereby generating enhanced mid-level stability. We compare the frequency and strength of these stable layers to those in other ocean basins utilizing data from other field campaigns. These comparisons highlight the correlation between vertically decreasing relative humidity and enhanced stable layers.

Chapter 1

Introduction

Stable layers in the mid-troposphere are theorized to play a significant role in the trimodal distribution of tropical convective clouds by inhibiting the vertical growth of convection and promoting high concentrations of cumulus congestus clouds (Lin and Johnson, 1996; Johnson et al., 1996; Zuidema, 1998; Johnson et al., 1999; Posselt et al., 2008; Spaulding-Astudillo and Mitchell, 2025). There are typically three layers of high stability in the tropical troposphere: a trade wind inversion, usually located at an altitude of 2 kilometers; a layer in the mid-levels, which has been documented to frequently occur near the 0°C level at altitudes around 5 km; and an inversion at the tropopause (Lin and Johnson, 1996; Johnson et al., 1996, 1999; Posselt et al., 2008). This mid-level stable layer is particularly intriguing because the mechanisms behind its formation are not well understood, and its role in affecting the vertical distribution of convective cloud-tops has been debated for decades (Mapes and Zuidema, 1996; Zuidema, 1998; Johnson et al., 1999; Spaulding-Astudillo and Mitchell, 2025). Consequently, considerable effort has been devoted to identifying the processes responsible for generating and maintaining this layer, leading to multiple competing hypotheses.

Several possible explanations for the formation of a tropical mid-level stable layer have been put forward. Johnson et al. (1996) propose that the direct thermal effects of melting may be sufficient to generate stable layers centered on the 0°C level. Additionally, both Mapes and Houze (1995) and Johnson et al. (1996) propose melting-driven convergence as one potential argument for the presence of a mid-level stable

layer observed during the Tropical Ocean-Global Atmosphere-Coupled Ocean Atmosphere Response Experiment (TOGA-COARE). Johnson et al. (1999) and Mapes and Zuidema (1996) further develop this hypothesis. They suggest that "melting convergence," driven by subsidence, could both draw in very dry air from subtropical latitudes and cool and moisten the column below the 0°C level. The resulting mid-level dryness could then lead to differential longwave cooling rates that act to further enhance stability across this layer (Mapes and Zuidema, 1996; Johnson et al., 1999). During TOGA-COARE, both the stable layer and the 0°C level were observed to be collocated, which supports this argument of melting-layer driven stability (Johnson et al., 1996, 1999). Strong dry layers have often been observed at similar altitudes, lending further credence to the relationship between mid-level dryness and mid-level stability (Mapes and Zuidema, 1996; Brown and Zhang, 1997; Zuidema, 1998; Johnson et al., 1999; Randel et al., 2016). Numerical modeling studies provide further support, especially to the potential role of longwave cooling gradients in helping to sustain a stable layer once formed (Posselt et al., 2008).

A different argument for the existence of mid-level stability comes from Spaulding-Astudillo and Mitchell (2025). They demonstrate that the number of longwave absorption lines in the water vapor spectral band decreases in the mid-troposphere, which results in a decrease in clear-sky longwave cooling rate from about 5–7 km. They hypothesize that this clear-sky cooling feature explains the prominence of congestus cloud tops around these levels by favoring divergence in convective regions in the same layer. Furthermore, they find that strong mid-level dryness enhances this longwave cooling gradient, consistent with the arguments of past studies (Mapes and Houze, 1995; Lin and Johnson, 1996; Johnson et al., 1996; Mapes and Zuidema, 1996; Johnson et al., 1999).

While it has long been proposed that strong mid-level stability is linked to vertical

humidity structures, in situ observations confirming this relationship in the tropical Atlantic remain limited, motivating targeted field measurements in this region. Observations from a recent field campaign enable us to revisit the governing mechanisms of these mid-level stable layers.

The Organized Convection and EarthCARE Studies over the Tropical Atlantic (ORCESTRA) field campaign was conducted from 8 Aug–30 Sept 2024, with the primary objectives of determining the drivers of mesoscale organization in the tropics and their impact on other weather systems, as well as to serve as a benchmark for satellite remote sensing and storm resolving models (Stevens et al., 2026). The campaign included a basin-wide sounding network (Gloeckner et al., 2025; Winkler et al., 2026) consisting of (1) radiosondes launched from ground stations on Cape Verde and Barbados contributed by the Mesoscale Organization of Tropical Convection (MAESTRO), Sub-Cloud Observations of Rain Evaporation (SCORE), Persistent EarthCARE Underflight Studies of the ITCZ and Organized Convection (PERCUSION), and Process Investigation of Clouds and Convective Organization over the atLantic Ocean (PICCOLO) sub-campaigns (Gloeckner et al., 2025; Stevens et al., 2026; Wing et al., 2026); (2) radiosondes launched from the RV Meteor ship as it traversed the Atlantic between Cape Verde and Barbados as part of the Beobachtung von Ozean und Wolken – Das Trans ITCZ Experiment (BOWTIE) and PICCOLO sub-campaigns (Klocke et al., 2026; Wing et al., 2026); and (3) dropsondes launched by a high altitude aircraft (HALO) (Stevens et al., 2026) both near Cape Verde and near Barbados in association with the PERCUSION sub-campaign (Groß et al., 2026). The PICCOLO and BOWTIE sub-campaigns were both primarily based on the R/V Meteor, which traversed the tropical Atlantic from Cabo Verde to Barbados over the duration of the campaign (Klocke et al., 2026).

Motivated by the prior literature, we hypothesize that there is an important positive

feedback between mid-level humidity gradients and high static stability. Here we use the ORCESTRA sounding dataset to investigate the structure and frequency of these stable layers in the tropical Atlantic, to compare with other field campaigns in other seasons and tropical ocean basins, and to revisit existing hypotheses concerning their origin mechanisms. We will present Mechanism-denial experiments using calculated radiative heating rates with and without this moisture gradient, which demonstrate that the presence of such a gradient is sufficient to generate radiatively-induced mid-level stable layers.

Chapter 2

Data and Methods

The majority of data used in our analysis were collected during the ORCESTRA field campaign. All ORCESTRA analysis in this paper is based on radiosondes and dropsondes launched from aircraft, ship, and island platforms, which are described in detail by Gloeckner et al. (2025) and Winkler et al. (2026). We specifically leverage radiosondes launched from the Barbados Cloud Observatory, the Ocean Science Center Mindelo (OSCM) in Cabo Verde, and the R/V Meteor as part of the RAPSODI sounding collection. We include 141 soundings launched from the BCO, 156 from the OSCM, and 322 from the R/V Meteor, for a total of 619 radiosondes. We also utilize 976 dropsondes released from the HALO aircraft, which operated out of both Cabo Verde and Barbados as part of the PERCUSION sub-campaign (Gloeckner et al., 2025). This results in a combined ORCESTRA dataset consisting of 1595 quality-controlled soundings.

We include further analysis on radiosonde and dropsonde datasets from other tropical oceanic field campaigns for the purpose of comparing trends across other seasons and ocean basins. Data from 1073 radiosondes launched during the Dynamics of the Madden Julian Oscillation (DYNAMO) campaign are utilized, specifically from the R/V Relleve the R/V Mirai, as well as from the islands of Gan and Diego Garcia (Ciesielski et al., 2014). DYNAMO was conducted in the tropical Indian Ocean from Oct 2011–Mar 2012. We also examine data from 647 dropsondes launched during the Organization of Tropical East Pacific Convection (OTREC) campaign, which was conducted from Aug–Sept 2019. OTREC took place in the tropical East Pacific, which

thus provides us insight into how the occurrence of mid-level stable layers varies across tropical ocean basins. Finally, we look at data collected from 1108 balloon soundings and dropsondes during the ElUcidating the RolE of Clouds-Circulation Coupling in ClimAte (EUREC^{4}A) campaign Stevens et al. (2021); Vömel et al. (2021); Stephan et al. (2021). The EUREC^{4}A campaign occurred in a similar location to ORCESTRA, with Barbados as its main base of operations. However, it was conducted from Jan–Feb 2020, providing a seasonal contrast to ORCESTRA.

In addition to the quality control that each of these datasets were already subjected to (Gottschalck et al., 2013; Ciesielski et al., 2014; Stevens et al., 2021; Stone et al., 2025; Gloeckner et al., 2025; Winkler et al., 2026), we undertook additional steps to ensure that no soundings with significant amounts of missing values were included in our analysis. Any sounding with more than 10% of mixing ratio or temperature values missing below 10 km or that contained a streak of missing values 100 m or longer below 10 km was excluded from our analysis. For all sounding datasets, relative humidity values were calculated from water vapor specific humidity with respect to ice, where the temperature was less than 0°C. For each sounding, a 100 m rolling mean smoother was applied to θ, $d\theta/dz$, and relative humidity to reduce noise.

In order to quantify the magnitude of mid-level stability events, we developed an empirical stability index (ς). This index enables empirical comparisons between different soundings and datasets, and allows for statistical analysis of the relationship between high stability and other variables of interest. ς in $K\ km^{-1}$ for a given sounding is defined as the difference between the maximum $d\theta/dz$ and the mean $d\theta/dz$ in the 4-8 km layer. According to Holton and Hakim (2013), $d\theta/dz$ is an established metric for static stability, and the 4-8 km layer was chosen as it fully encompasses the layer typically occupied by mid-level stable layers without including the trade wind inversion or the tropopause (Johnson et al., 1999; Posselt et al., 2008).

Chapter 3

Results

3.1 Initial Sounding Observations and CFADs

Scientists aboard the R/V Meteor during ORCESTRA noticed a higher prevalence of congestus clouds and fewer cumulonimbus than expected, based on subjective visual observations. Inspection of the sounding data revealed the frequent occurrence of remarkably strong mid-level stable layers, with an example provided in Fig. 3.1a. The trade wind inversions described in previous literature (Johnson et al., 1996, 1999) are also visible at altitudes of ∼1.7 km and near a temperature of 17°C.

Fig. 3.1b and Fig. 3.1c demonstrate that these mid-level stable layers maximize around –5°C and ∼6 km, instead of the 0°C level located around 5 km described previously. It is also apparent from both Fig. 3.1a and Fig. 3.1b that these layers of strong mid-level stability are associated with rapid vertical drying. Notably, the contoured frequency by altitude diagram (CFAD) of relative humidity (Fig. 3.1d) is dominated by moist values below the 6.1 km line and a much broader distribution and drier mean values above. This supports the hypothesis that there is a positive feedback between mid-level humidity gradients and high static stability.

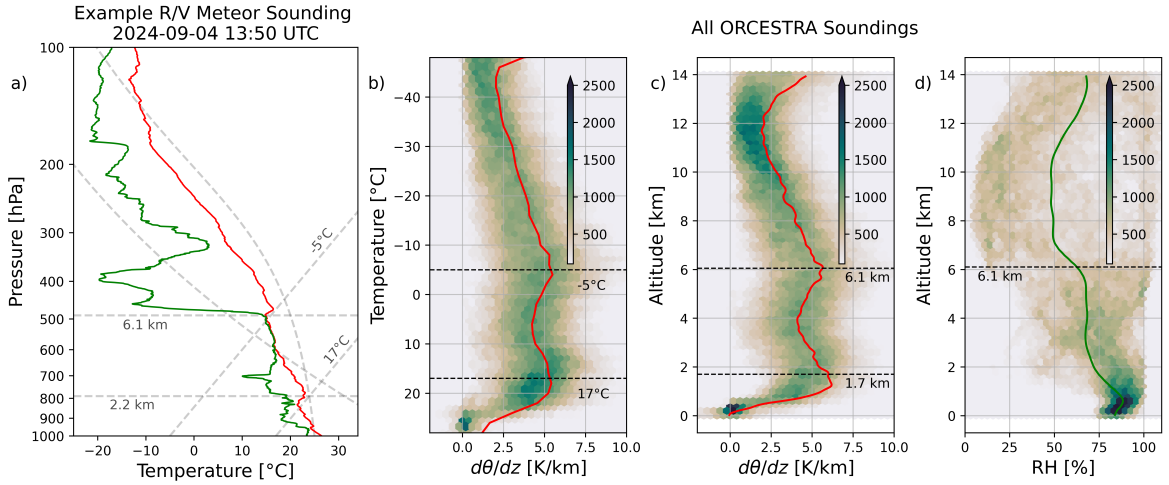


Figure 3.1: a) Example Skew–T log–P diagram taken from the R/V Meteor during ORCESTRA, showing a strong mid-level stable layer (inversion) and a rapid decrease in humidity across that layer (∼6 km). b) CFAD of $d\theta/dz$ with temperature as the vertical coordinate for all ORCESTRA soundings. The mean $d\theta/dz$ is shown in red. c) Same as b), but with altitude as the vertical coordinate. d) CFAD of relative humidity for all ORCESTRA soundings. The mean relative humidity profile is shown in green. Dashed lines in the CFADs correspond to local maxima objectively identified, a selection of which are incorporated into the Skew–T.

3.2 The Relationship with Humidity

As seen in Figure 3.1, the ORCESTRA-mean profile of relative humidity exhibits a dramatic decrease in humidity that occurs at the same altitude and temperature as the mid-level peak in stability. To quantify this relationship, we calculated both ς and the relative humidity difference across the mid-level stable layer for each sounding taken during ORCESTRA. Mapes and Zuidema (1996) refer to this concept of rapid vertical drying as *humidity drops*, but we refer to our quantified version as the *relative humidity layer difference*. To calculate this difference, we first identify the altitude of maximum $d\theta/dz$ (z_{max}) within the 4-8 km layer. We then compute the mean relative humidity in two layers. These layers are 330 meters deep, and are displaced by 50 meters above and below z_{max}. We then take the difference between these two mean

values, with negative values indicating drier air above the stable layer.

Figure 3.2 visualizes the relationship between ς and the relative humidity layer difference using a scatter plot constructed from all available ORCESTRA soundings. Each point represents an individual profile, and a linear least-squares regression was applied to the paired values to quantify their covariability. The resulting fit indicates a statistically robust inverse relationship ($p < 0.0001$), with increasing stability corresponding to progressively more negative relative humidity layer differences. This behavior is consistent with enhanced stratification coinciding with a sharper transition to drier air above the stable layer. Furthermore, the most extreme stability events (with $\varsigma > 15$ K km^{-1}) are exclusively associated with strongly negative relative humidity layer differences, reinforcing the interpretation that pronounced stability is systematically linked to a substantial decrease of humidity across the sampled profiles. Some examples of these soundings from the ORCESTRA campaign can be seen in Fig. 3.3. This strong relationship between ς and negative relative humidity layer differences provides support to the hypothesis of Johnson et al. (1999) and Mapes and Zuidema (1996) that strong humidity gradients promote differential longwave cooling rates and thus the formation and/or maintenance of mid-level stable layers.

The same scatterplots were also generated for the DYNAMO, OTREC, and EUREC4A field campaigns, with similar results (see Figs. 3.4 - 3.6). Despite some differences in the shape of the distributions, all of the field campaigns exhibit the same statistically robust inverse relationship between relative humidity layer differences and high stability events ($p < 0.0001$ for all calculated slopes). The consistency of this relationship across field campaigns indicates that the relationship is likely independent of environmental conditions unique to any given ocean basin or time period, and is instead a more fundamental attribute of mid-level stability across the tropical world.

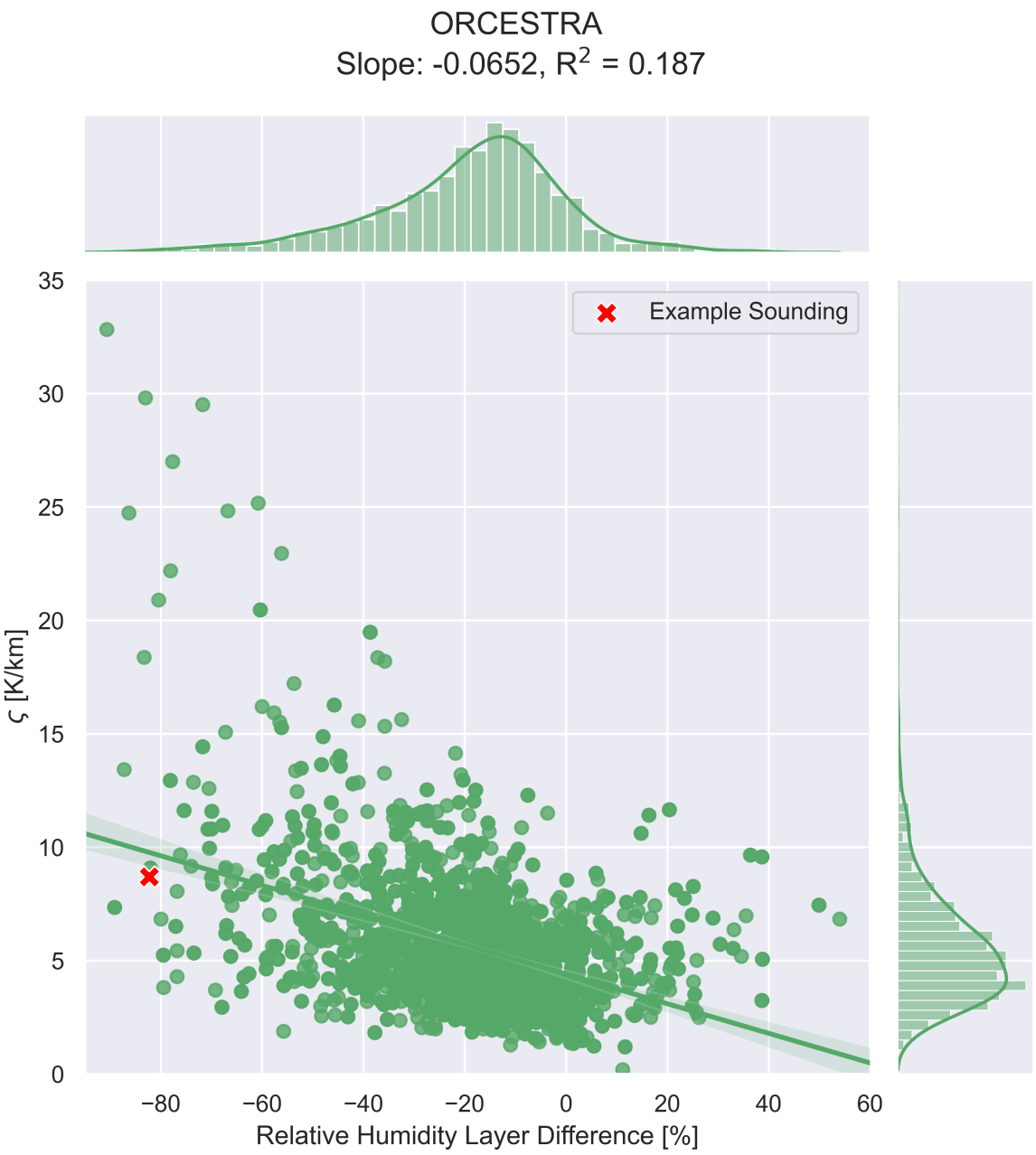


Figure 3.2: Scatter plot of the relationship between relative humidity layer difference (%) and the stability index ς (in K/km) for ORCESTRA observations. Each green point represents an individual measurement, with histograms along the margins showing the distributions of both variables. Negative relative humidity layer difference values indicate drier air above the stable layer. The "Example Sounding" denotes the sounding used in Figs. 3.1 and 3.8.

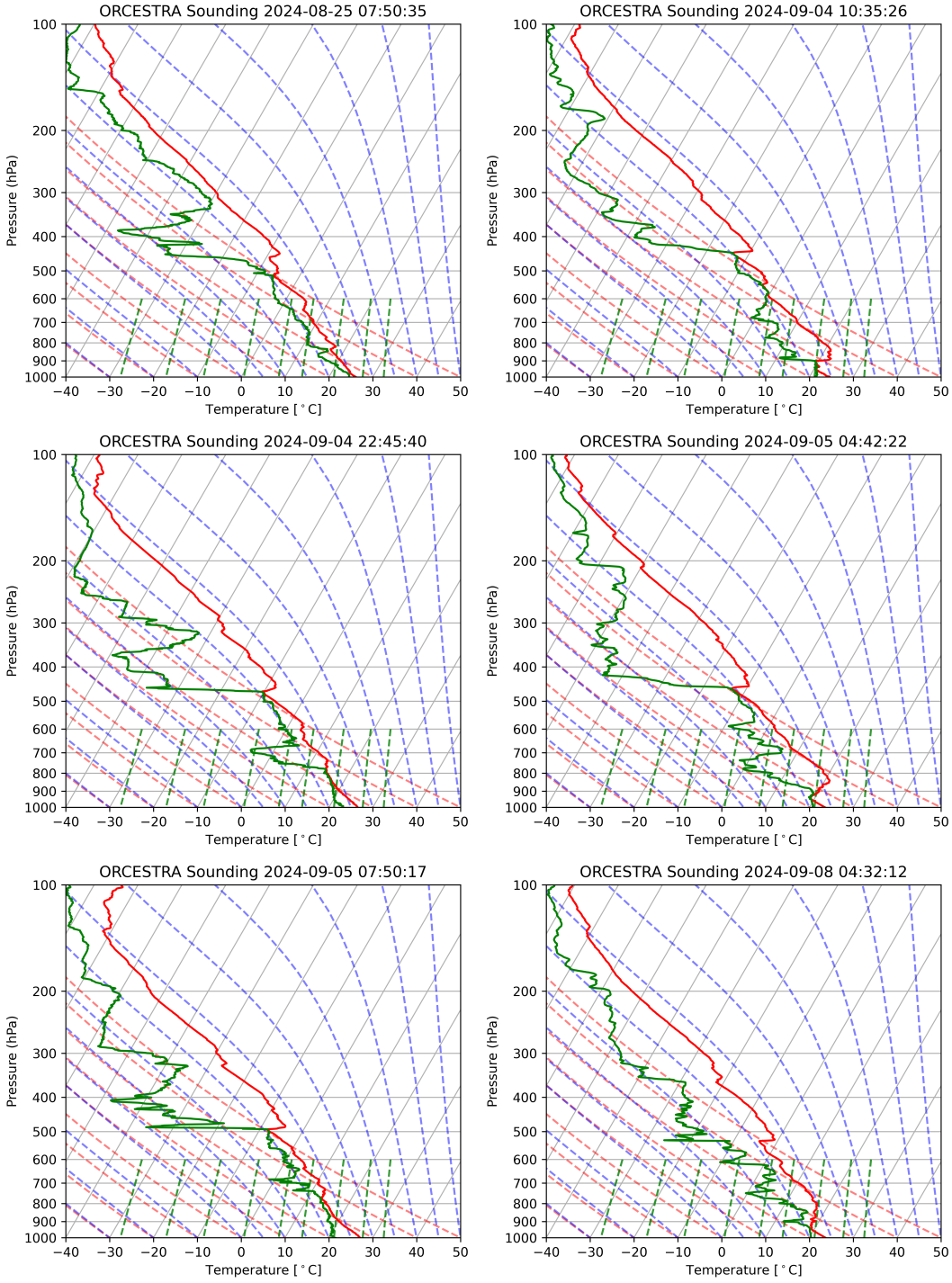


Figure 3.3: A selection of soundings with extremely strong mid-level stable layers from the ORCESTRA campaign. All soundings featured have values of $\varsigma \geq 15$ K km^{-1}. Note the presence of mid-level rapid vertical drying collocated with strong static stability in all soundings.

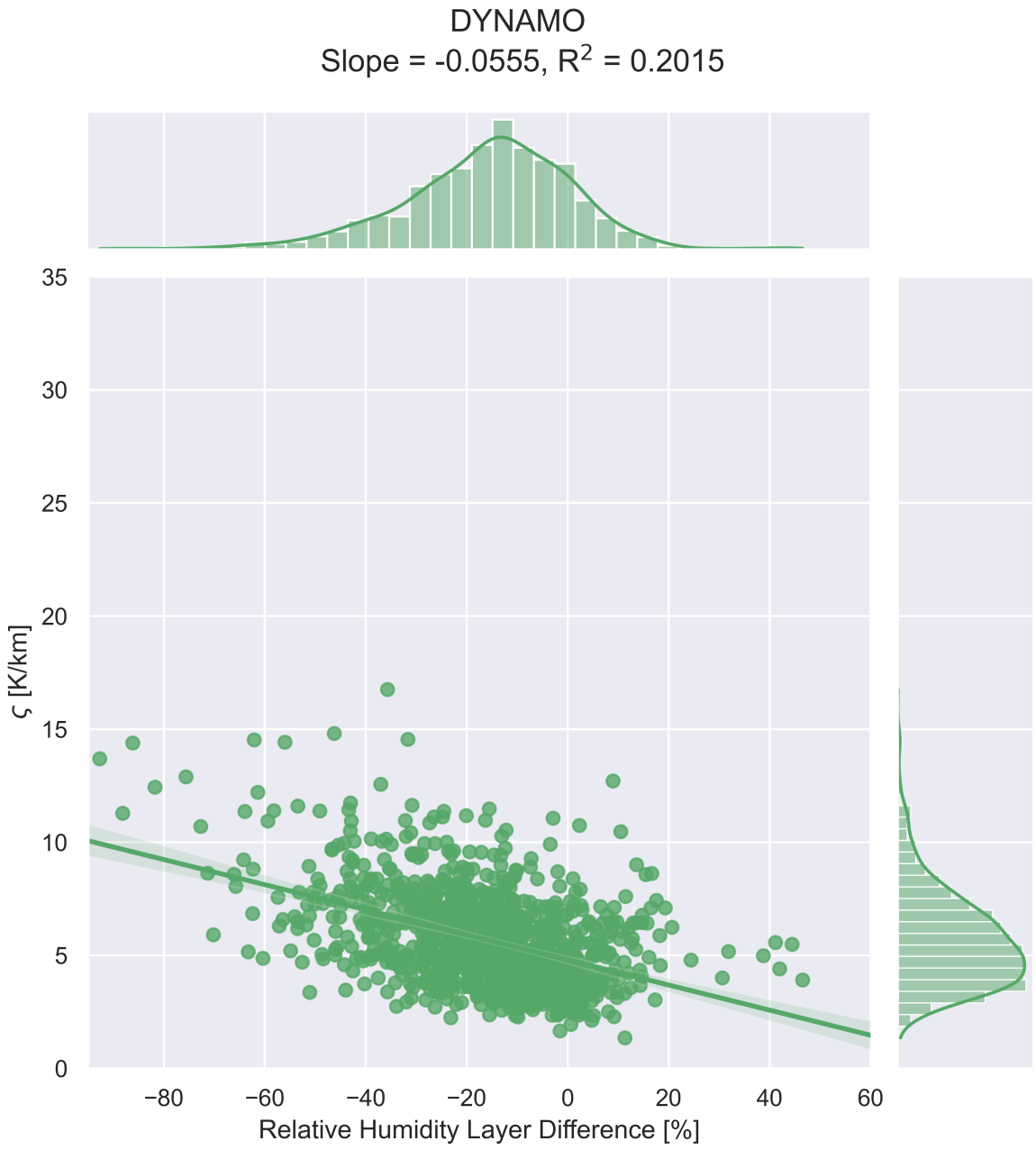


Figure 3.4: Same as Fig. 3.2, but for the DYNAMO campaign and without an example sounding.

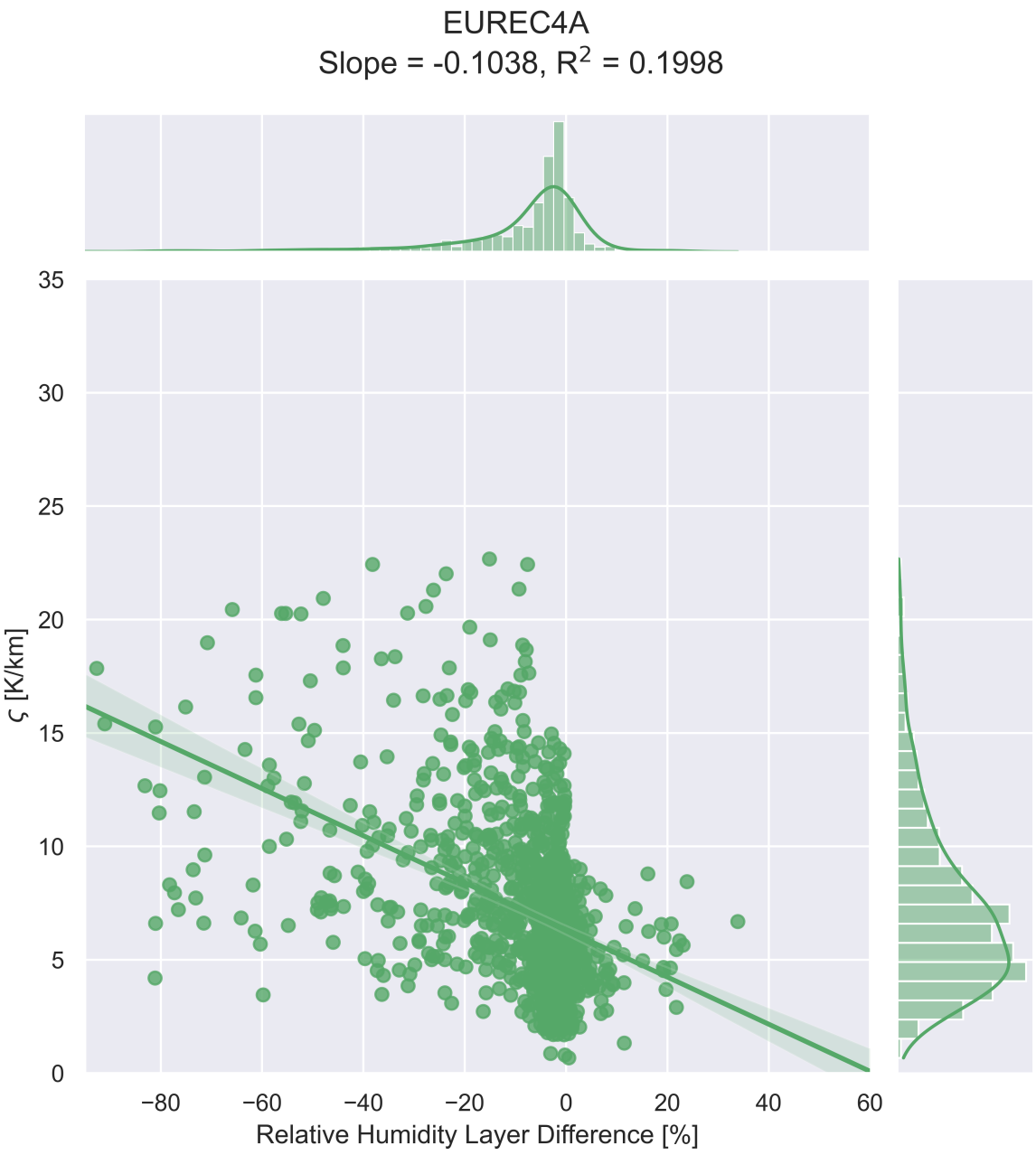


Figure 3.5: Same as Fig. 3.4, but for the EUREC^{4}A campaign.

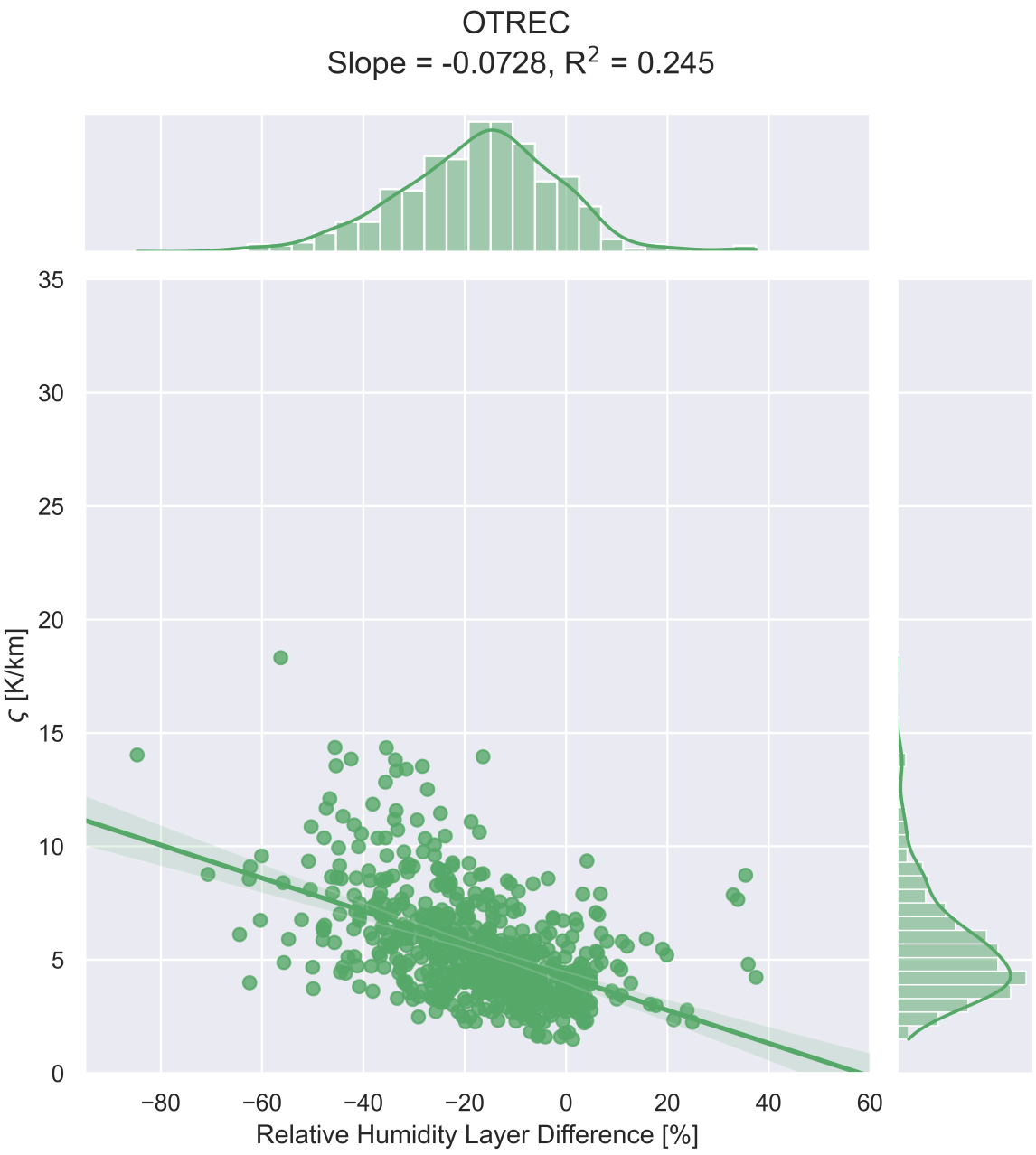


Figure 3.6: Same as Fig. 3.4, but for the OTREC campaign.

3.3 Comparison of Stable Layer Occurrence Across Campaigns

To illustrate and quantify the vertical distribution of stable layers and compare across the different field campaigns, we devised a modified categorical version of ς. Instead of using the 4-8 km layer (as in Figure 3.2), we allow the altitude of the layer to vary and restrict the width to 2 km. Stable layers are identified in a sounding by computing this new stability index every 500 meters throughout the entire sounding. If this value exceeds 8 K km^{-1}, then a stable layer event is recorded in that sounding for that altitude. This 8 K km^{-1} value was chosen based on the value of $\overline{\varsigma} + 1\sigma = 8.93$ K km^{-1} for the set of all ς values in the ORCESTRA campaign, where $\overline{\varsigma}$ and σ are the mean and standard deviation, respectively. The frequency of stable layer events were recorded for each altitude across all field campaigns and plotted in Fig. 3.7.

The ORCESTRA distribution exhibits high stable layer frequency within a few kilometers of the surface, likely associated with the trade wind inversion (Fig. 3.7a). There is also an expected peak in stable layer frequency centered around 6 km, supporting the high occurrence of mid-level stable layer events for the campaign (Fig. 3.1). The OTREC distribution has a similar structure to that of ORCESTRA, with the same trade wind peak and a relatively well-defined peak in the mid-levels. DYNAMO also features a strong mid-level stability feature, but it is noticeably displaced above the other field campaigns. Interestingly, the EUREC^{4}A distribution displays much higher stable layer frequencies at all altitudes, while still displaying a roughly bimodal distribution (likely trimodal if the tropopause was included). This could be related to the difference in season between EUREC^{4}A and ORCESTRA. As noted by Casey et al. (2009), dry layers occur more frequently in the winter, potentially contributing to the

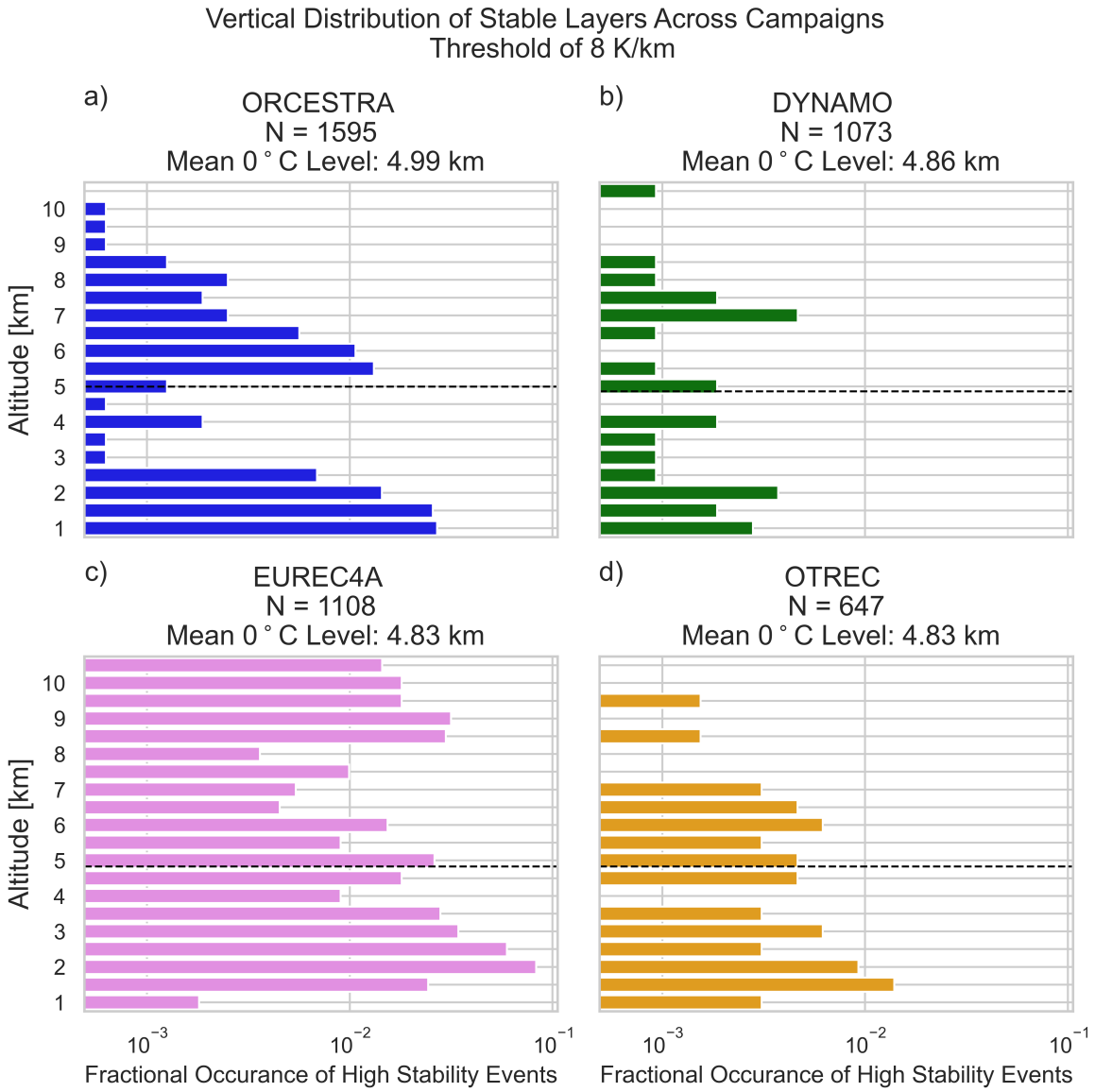


Figure 3.7: Vertical distribution of high-stability atmospheric layers across four field campaigns. Horizontal bars show the occurrence frequency of stable layers at different altitudes between 1–10 km, as occurrence normalized by total number of soundings (shown as N). The vertical axis is limited to 10 km since dropsonde datasets frequently lack data above this level.

greater frequency of high stability events observed in EUREC^{4}A. These differences in the distributions between the four campaigns remain unexplained. There is likely variability in the origin and strength of dry layers between tropical ocean basins, but further research is required to uncover the nature of these differences.

All four field campaigns display significant populations of stable layers at altitudes significantly above the 0°C level. This indicates that latent-heating related processes are not necessary for the development of these mid-level stable layers. While this does not imply that phase changes are unimportant for either creating or maintaining stable layers in some settings, it does require an alternative explanation in the case of the observed stable layers. As shown below, rapid vertical drying likely plays a critical role in their formation through interactions with longwave radiative heating rates.

3.4 Mechanism-Denial Testing With a Radiative Transfer Model

While the observed correspondence between relative humidity layer differences and high mid-level stability has now been established, we next seek to test the hypothesis that strong vertical humidity gradients alone are sufficient to produce mid-level stable layers through clear-sky radiative forcing, without the need for latent-heat related effects. To this end, we employ the Rapid Radiative Transfer Model for GCM Applications (RRTMG) as a single-column model to test the impact of high relative humidity layer differences on temperature, and hence $d\theta/dz$, through longwave heating rates. The RRTMG wrapper in the CLIMLAB Python package Rose (2018) was utilized for all RRTMG calculations, with no clouds included in the calculations. We include the shortwave heating rate in this analysis for completeness, although longwave cooling highly dominates over shortwave in the mean.

A mechanism-denial experiment was designed to explicitly demonstrate the relationship between the strength of the vertical humidity decrease and mid-level stability using the radiative transfer model. This experiment is loosely based on methodologies employed by Mapes and Zuidema (1996) and Fildier et al. (2023). However, we place a greater emphasis on both the isolation of humidity and temperature effects and the importance of gradients of these variables across the stable layer. First, we calculated profiles of longwave and shortwave radiative heating rates for a representative sounding with a well defined stable layer. We chose the sounding launched from the R/V Meteor on September 4th at 13:50 UTC during the ORCESTRA campaign, which is the sounding depicted in Fig. 3.1a. This sounding features a notable peak in mid-level stability collocated with a rapid decrease in humidity with altitude across the stable layer. The heating rates calculated directly from this sounding serve as a control case against which the results of the mechanism-denial tests are directly compared.

We next conduct two tests to isolate the effects of the strong humidity gradient. We specifically test the impact of removing either the rapid humidity decrease or the existence of the stable layer, itself, by selectively smoothing either the temperature profile or the mixing ratio profile across the stable layer and comparing the resulting heating rate profiles for these two scenarios to the control. The temperature and mixing ratio profiles were first heavily smoothed by applying a 1-km rolling mean smoother. However, the part of the profile surrounding the stable layer was selectively preserved, keeping only the sharp mixing ratio gradient for the first experiment (Fig. 3.8b), and keeping the same part of the temperature profile for the second (Fig. 3.8c). The radiative tendencies were then calculated from these profiles. This allows us to test the effects of humidity versus temperature on longwave heating rates separately. Fig 3.8b also includes the effect of imposing the calculated net heating rate back on to the potential temperature profile.

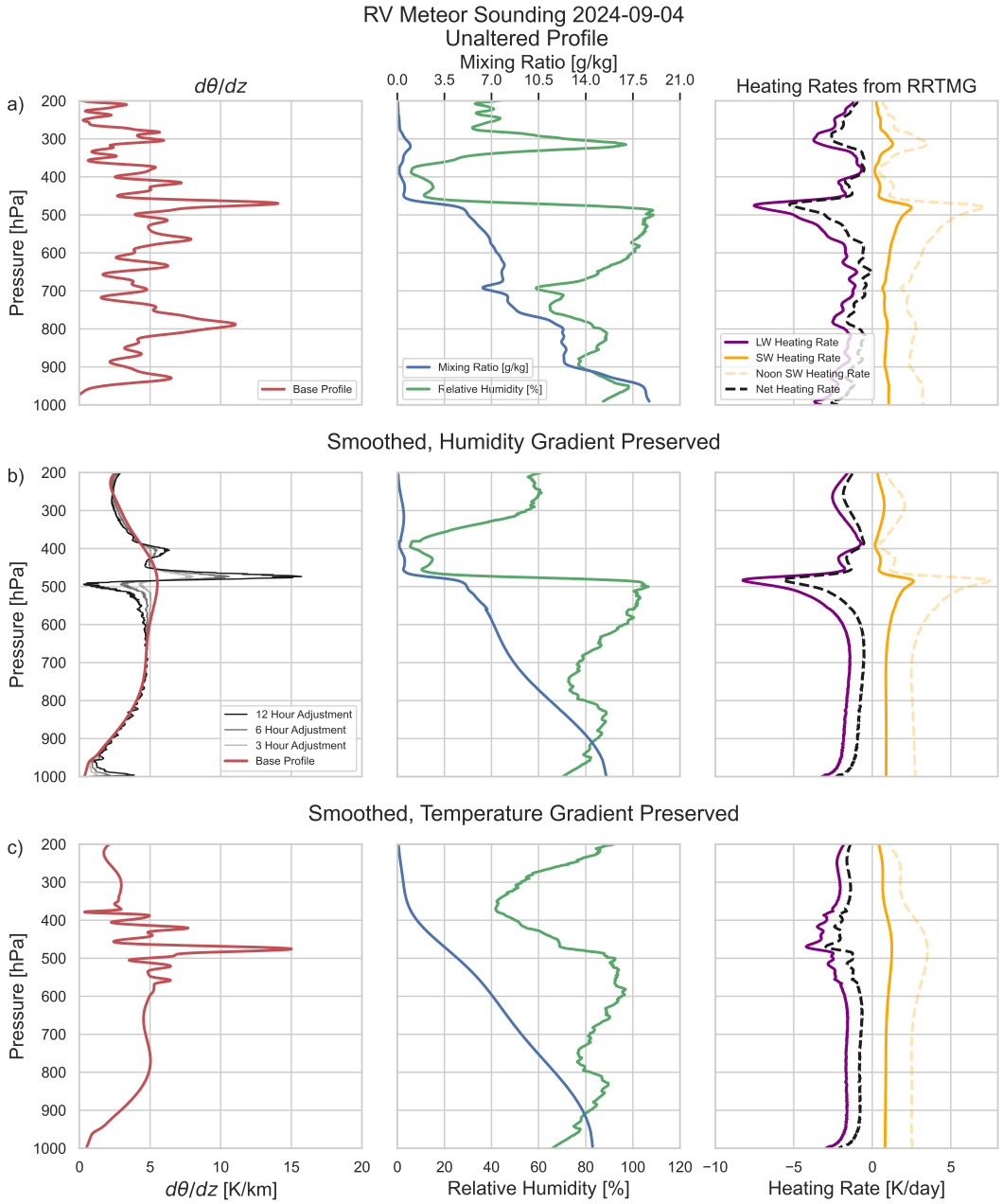


Figure 3.8: Vertical profiles from mechanism denial experiments using the example R/V Meteor sounding from Fig. 3.1a. The left column shows $d\theta/dz$, the middle column displays relative humidity in green and mixing ratio in blue, and the right column shows longwave, shortwave, and net heating rates calculated by RRTMG. The solid yellow line indicates the shortwave heating rate averaged over a 24 hour period of solar angles. Row a) shows these values for the unaltered sounding profile. Row b) shows these profiles for heavily smoothed temperature and humidity profiles, but with the humidity structure near the stable layer preserved. It also shows the impact of imposing the net heating rate onto the smoothed potential temperature profile. Row c) is the same, but with the temperature structure preserved instead.

It is immediately apparent from Fig. 3.8b that a strong humidity gradient is the primary driver of enhanced longwave cooling near the region of enhanced stability. The shape of the longwave heating rate profile is nearly identical to that in Fig. 3.8a, with a well-defined peak coincident with the location of the stable layer. In contrast, the peak in longwave cooling near the stable layer in Figure 3.8c is substantially dampened. The same can be said of the peak in the shortwave heating rate: the magnitude of this peak strongly depends on the magnitude of this humidity gradient.

Profiles with 3-, 6-, and 12-hour adjustments of $d\theta/dz$ were calculated and are shown in Fig. 3.8b. To calculate these profiles, we first impose the net heating rate profile (indicated by the dashed black line in the rightmost column) onto the heavily smoothed temperature profile of the sounding, adjusted from K/day to K/hour and multiplied accordingly. θ and $d\theta/dz$ were then recalculated from these adjusted temperature profiles. The shape of these adjusted $d\theta/dz$ profiles strongly resemble the shape of the $d\theta/dz$ profile in Fig. 3.8c, and indicates that the cooling rates induced by the humidity gradient are sufficient to generate a strong mid-level stable layer over a sub-daily timescale. Specifically, the humidity gradient we tested radiatively induced a stable layer with $\varsigma \geq 8$ K km^{-1} in just ten hours.

The entirety of this experiment was repeated for other representative soundings from the ORCESTRA dataset with similar results (not shown). This experiment confirms that the existence of a strong vertical humidity gradient associated with mid-level dryness for less than a day is sufficient to induce a high mid-level stability event. Furthermore, it shows that the presence of a stable layer is not sufficient to generate the cooling rates required to sustain itself without the presence of a strong vertical humidity gradient.

Chapter 4

Summary and Conclusions

In this study, we document the frequent occurrence of mid-level stable layers near 6 km during the ORCESTRA campaign, which is in contrast to the typical picture of stability maxima collocated with the 0°C level. Analysis of radiosonde observations demonstrates a consistent and statistically robust relationship between enhanced static stability and negative relative humidity layer differences across the stable layer (drier above), a result that is reproduced across multiple field campaigns spanning different tropical ocean basins and is in agreement with prior studies (Mapes and Houze, 1995; Lin and Johnson, 1996; Johnson et al., 1996; Mapes and Zuidema, 1996; Johnson et al., 1999; Spaulding-Astudillo and Mitchell, 2025). This consistent relationship suggests that the coupling between vertical moisture structure and enhanced static stability represents a fundamental aspect of tropical atmospheric thermodynamics rather than a regionally specific phenomenon.

Mechanism denial experiments using a single-column longwave radiative transfer model (RRTMG) further indicate that sharp vertical humidity gradients observed during ORCESTRA are sufficient to generate localized maxima in longwave cooling, providing a pathway for the development and maintenance of mid-level stable layers in less than a day. Specifically, the presence of dry air aloft enhances radiative cooling from the top of the moist layer, reinforcing vertical stratification and promoting the formation of elevated stability maxima. Furthermore, comparison between ORCESTRA, DYNAMO, OTREC, and EUREC^{4}A demonstrates that elevated stable layers

are a more common feature of the tropical atmosphere than has been documented previously, occurring in each of these datasets and frequently at altitudes well above the 0°C level.

Our results highlight the need for accurate representation of humidity gradients and their influence on radiative heating in numerical weather models, to the extent that these feedbacks strongly affect the depth and organization of tropical convection. Horizontal advection of dry air from continental or subtropical regions has been hypothesized as the source of these humidity gradients (Mapes and Houze, 1995; Johnson et al., 1996; Mapes and Zuidema, 1996; Johnson et al., 1999), but the precise sources and transport pathways of these air masses and their potential links to mid-level stable layers remain uncertain. Parcel trajectory analyses could potentially help disentangle these contributions and identify dominant source regions across different basins. Additionally, there remains the question of if and how both congestus clouds and thin layer-clouds feed back upon these mid-level stable layers. Radiatively driven stability may favor detrainment at specific levels, promoting the persistence of congestus cloud populations, which in turn reinforce the humidity gradients that initially generated the stable layer through differential moistening and drying. Additional research on such topics would help determine whether the observed trimodal cloud distribution in the tropics emerges from this two-way interaction between clouds and radiatively maintained stability structures.

Reference List

Brown, R. G., and C. Zhang, 1997: Variability of midtropospheric moisture and its effect on cloud-top height distribution during toga coare. *Journal of the Atmospheric Sciences*, **54 (23)**, 2760–2774, https://doi.org/10.1175/1520-0469(1997)054⟨2760:VOMMAI⟩2.0.CO;2.

Casey, S. P. F., A. E. Dessler, and C. Schumacher, 2009: Five-year climatology of midtroposphere dry air layers in warm tropical ocean regions as viewed by airs/aqua. *Journal of Applied Meteorology and Climatology*, **48 (9)**, 1831–1842, https://doi.org/10.1175/2009JAMC2099.1.

Ciesielski, P. E., and Coauthors, 2014: Quality-controlled upper-air sounding dataset for dynamo/cindy/amie: Development and corrections. *Journal of Atmospheric and Oceanic Technology*, **31 (4)**, 741–764, https://doi.org/10.1175/JTECH-D-13-00165.1.

Fildier, B., C. Muller, R. Pincus, and S. Fueglistaler, 2023: How moisture shapes low-level radiative cooling in subsidence regimes. *AGU Advances*, **4 (3)**, e2023AV000 880, https://doi.org/10.1029/2023AV000880.

Gloeckner, H. M., and Coauthors, 2025: Beach: Barbados and eastern atlantic combined high-altitude dropsonde datasets. *Earth System Science Data Discussions*, 1–35, https://doi.org/10.5194/essd-2025-647.

Gottschalck, J., P. E. Roundy, C. J. Schumacher, A. Vintzileos, and C. Zhang, 2013: Large-scale atmospheric and oceanic conditions during the 2011–12 dynamo field campaign. *Monthly Weather Review*, **141 (12)**, 4173–4196, https://doi.org/10.1175/MWR-D-13-00022.1.

Groß, S., and Coauthors, 2026: The earthcare validation campaign eva: combining aircraft and satellite observations for aerosol, cloud, and radiation measurements. *Atmospheric Measurement Techniques*, **19**, 3933–3959, https://doi.org/10.5194/amt-19-3933-2026.

Holton, J. R., and G. J. Hakim, 2013: The thermodynamic equation. *An Introduction to Dynamic Meteorology*, 5th ed., Academic Press, chap. 2, https://doi.org/10.1016/C2009-0-63394-8.

Johnson, R. H., P. E. Ciesielski, and K. A. Hart, 1996: Tropical inversions near the 0°c level. *Journal of the Atmospheric Sciences*, **53 (13)**, 1838–1855, https://doi.org/

10.1175/1520-0469(1996)053⟨1838:TINTL⟩2.0.CO;2.

Johnson, R. H., T. M. Rickenbach, S. A. Rutledge, P. E. Ciesielski, and W. H. Schubert, 1999: Trimodal characteristics of tropical convection. *Journal of Climate*, **12 (8)**, 2397–2418, https://doi.org/10.1175/1520-0442(1999)012⟨2397:TCOTC⟩2.0.CO;2.

Klocke, D., and Coauthors, 2026: 40 days and nights in the rains: The inner life of the atlantic itcz during bowtie. *Bulletin of the American Meteorological Society*, https://doi.org/10.1175/BAMS-D-25-0166.1, published online 4 June 2026.

Lin, X., and R. H. Johnson, 1996: Kinematic and thermodynamic characteristics of the flow over the western pacific warm pool during toga coare. *Journal of the Atmospheric Sciences*, **53 (5)**, 695–715, https://doi.org/10.1175/1520-0469(1996)053⟨0695:KATCOT⟩2.0.CO;2.

Mapes, B. E., and R. A. Houze, 1995: Diabatic divergence profiles in western pacific mesoscale convective systems. *Journal of the Atmospheric Sciences*, **52 (10)**, 1807–1828, https://doi.org/10.1175/1520-0469(1995)052⟨1807:DDPIWP⟩2.0.CO;2.

Mapes, B. E., and P. Zuidema, 1996: Radiative-dynamical consequences of dry tongues in the tropical troposphere. *Journal of the Atmospheric Sciences*, **53 (4)**, 620–638, https://doi.org/10.1175/1520-0469(1996)053⟨0620:RDCODT⟩2.0.CO;2.

Posselt, D. J., S. C. van den Heever, and G. L. Stephens, 2008: Trimodal cloudiness and tropical stable layers in simulations of radiative convective equilibrium. *Geophysical Research Letters*, **35 (8)**, L08 802, https://doi.org/10.1029/2007GL033029.

Randel, W. J., L. Rivoire, L. L. Pan, and S. B. Honomichl, 2016: Dry layers in the tropical troposphere observed during contrast and global behavior from gfs analyses. *Journal of Geophysical Research: Atmospheres*, **121 (23)**, 14 142–14 158, https://doi.org/10.1002/2016JD025841.

Rose, B. E. J., 2018: Climlab: a python toolkit for interactive, process-oriented climate modeling. *Journal of Open Source Software*, **3 (24)**, 659, https://doi.org/10.21105/joss.00659.

Spaulding-Astudillo, F. E., and J. L. Mitchell, 2025: Clear-sky convergence, water vapor spectroscopy, and the origin of tropical congestus clouds. *AGU Advances*, **6 (1)**, e2024AV001 300, https://doi.org/10.1029/2024AV001300.

Stephan, C. C., and Coauthors, 2021: Ship- and island-based atmospheric soundings from the 2020 eurec4a field campaign. *Earth System Science Data*, **13 (2)**, 491–514, https://doi.org/10.5194/essd-13-491-2021.

Stevens, B., S. Bony, and Coauthors, 2021: Eurec4a. *Earth System Science Data*, **13 (8)**, 4067–4119, https://doi.org/10.5194/essd-13-4067-2021.

Stevens, B., and Coauthors, 2026: Orcestra: Organized convection and earthcare studies over the tropical atlantic. *Tellus*, **79 (1)**, https://doi.org/10.16993/tellus.4123.

Stone, Z., and Coauthors, 2025: The organization of tropical east pacific convection (otrec) field campaign—five years later. *Bulletin of the American Meteorological Society*, **106 (7)**, E1264–E1275, https://doi.org/10.1175/BAMS-D-24-0134.1.

Vömel, H., and Coauthors, 2021: High-resolution in situ observations of atmospheric thermodynamics using dropsondes during the organization of tropical east pacific convection (otrec) field campaign. *Earth System Science Data*, **13 (3)**, 1107–1117, https://doi.org/10.5194/essd-13-1107-2021.

Wing, A. A., and Coauthors, 2026: Piccolo: Process investigation of clouds and convective organization over the atlantic ocean. *Bull. Amer. Meteor. Soc., in review.*

Winkler, M., and Coauthors, 2026: Rapsodi: Radiosonde atmospheric profiles from ship and island platforms during orcestra, collected to decipher the itcz. *Earth System Science Data*, **18 (3)**, 1833–1854, https://doi.org/10.5194/essd-18-1833-2026.

Zuidema, P., 1998: The 600–800-mb minimum in tropical cloudiness observed during toga coare. *Journal of the Atmospheric Sciences*, **55 (12)**, 2220–2228, https://doi.org/10.1175/1520-0469(1998)055⟨2220:TMMITC⟩2.0.CO;2.